# 6.4 Role of Cations in RNA Folding and Function

*Jessica C. Bowman, Anton S. Petrov, and Loren Dean Williams*

## CONTENTS



### 6.4.1 CATIONS IN WATER: RELEVANCE TO ORIGIN OF LIFE AND EVOLUTION ON EARTH

Inorganic metal cations are abundant in cells and are essential to life on Earth. Metal cations are vital for a variety of biological processes. Fundamental biological processes such as electron transfer, photosynthesis, and respiration require these ions (Bertini et al. 2007). Cations stabilize transition states in the replication of DNA, transcription of DNA to RNA, and ligation and cleavage of the nucleic acids by both proteins and ribozymes (Lykke-Andersen and Christiansen 1998; Steitz 1999; Doherty and Dafforn 2000; Lee et al. 2000; Yin and Steitz 2004; Ellenberger and Tomkinson 2008). Protein sequences encoded in messenger RNA are translated by amino-acid-bearing tRNAs at the ribosome, neither of which are transcribed, folded, assembled, or functional in the absence of inorganic cations. Few natural biological manipulations of the nucleic acid phosphodiester backbone proceed *in vitro* without divalent cations, and none are known to proceed in the absence of monovalent cations. Divalent cations stabilize three-dimensional structures of proteins, catalyze redox reactions, stabilize cell membranes, and transmit electrical current in the nervous system. Here, we focus on the interactions of metal ions with nucleic acids and explain their role in the translation system.

The earliest available data suggests that translation, one of the most central processes of life, originated with dependence on inorganic cations. The catalytic center of the ribosomal large subunit (LSU), responsible for peptide bond formation, is stabilized by $Mg^{2+}$. Within 20 Å of this center, about 20% of the phosphate oxygens of the RNA phosphodiester backbone interact directly with $Mg^{2+}$ (Klein et al. 2004; Hsiao et al. 2009). $Mg^{2+}$ bridges RNA nucleotides from disparate regions of the RNA sequence to form a structure that is inaccessible with monovalent cations alone (Hsiao and Williams 2009; Lenz et al. 2017). These $Mg^{2+}$-RNA bridges are highly conserved in position and structure through all three major evolutionary branches of life, suggesting that they preceded, or at least coincided with, the last universal common ancestor (LUCA).

The availability of biologically useful inorganic ions is dependent on the existence of certain minerals and on their solubility in water. The composition of the atmosphere affects cation solubility, especially partial pressures of $O_{2(g)}$ and $CO_{2(g)}$. An influx of $O_{2(g)}$ to an aqueous system diminishes the solubility of redox-sensitive ions such as $Cu^{2+}$, $Fe^{2+}$, and $Mn^{2+}$. Similarly, $CO_{2(g)}$ decreases pH, mobilizing ions such as $Ca^{2+}$ and $Na^{+}$ from soils and precipitants. $Fe^{2+}$ has been proposed and demonstrated to be a functional early Earth analogue for $Mg^{2+}$ in nucleic-acid-processing steps, due to its similarity in size and charge density (Athavale et al. 2012; Okafor et al. 2017). Yet, in the pH range that sustains most life, $Fe^{2+}_{(aq)}$ precipitates as $Fe(OH)_{2(s)}$ (Morgan and Lahav 2007) or $Fe(III)_{(s)}$ species (Derry 2015) in a complex mechanism and at a rate that is dependent on the concentration of dissolved $O_{2(g)}$. Together with well-documented substitutions of $Cu^{2+}$, $Zn^{2+}$, and $Mn^{2+}$ for $Fe^{2+}$ in catalytic proteins (Torrents et al. 2002;

Wolfe-Simon et al. 2006; Anjem et al. 2009; Cotruvo and Stubbe 2011; Martin and Imlay 2011; Ushizaka et al. 2011; Aguirre and Culotta 2012; Harel et al. 2014), these observations suggest that changes in Earth's atmosphere over evolution may have altered the ions of key ion-dependent biological processes.

Water's interactions with ions are as important to biology as the ions themselves. Cations observed at the atomic level in three-dimensional molecular structures are almost always at least partially hydrated. Water molecules are coordinated, oriented, polarized, and acidified by ions in a manner that depends on the properties of the ion—mainly size and charge density (Hribar et al. 2002; Collins et al. 2007). Hydrated cations mitigate the negative charge on nucleic acids by long-range electrostatic and shorter-range hydrogen-bonding interactions with backbone phosphates. Partial dehydration allows direct coordination of the cation by phosphates (up to four for $Mg^{2+}$) of the nucleic acid backbone, while remaining cation-coordinated water molecules are available to participate in hydrogen bonding. Cation hydration mitigates the thermodynamic favorability of direct coordination by phosphodiesters by requiring unfavorable dehydration. Together, these interactions provide access to a range of complex and finely tunable conformational states of the RNA. The functional roles of cations in extant biology are interdependent with the unique properties of water.

## 6.4.2 HYDRATED CATIONS

### 6.4.2.1 Coordination by Water

Water molecules are oriented and polarized by cations, forming acidic metal hydrates $(Me(H_2O)_x)^{n+}$ with elevated potential for participation in hydrogen bonding and function in enzymatic activity and proton donation. The extent of attraction between a cation and water molecules is given by the cation's hydration enthalpy. A large, negative hydration enthalpy indicates a stronger attraction than a small, negative one. The hydration enthalpies of cations vary in magnitude by cation identity, roughly based on size and charge. Hydration enthalpies of $Zn^{2+}$ and $Mg^{2+}$, for example, are large in magnitude (~−450 kcal/mol) compared with those of $Na^{2+}$ and $K^{+}$ (~−100 kcal/mol) (Rashin and Honig 1985).

Biologically relevant metal hydrates include those of $Ca^{2+}$, $Fe^{2+}$, $K^{+}$, $Mg^{2+}$, $Mn^{2+}$, $Na^{+}$, and $Zn^{2+}$. These cations are coordinated by multiple water molecules in their hydrate form. The inherent polarity of each water molecule is increased by coordination with a cation, increasing the acidity of the water hydrogens. Experimentally derived $pK_a$s (Table 6.4.1) indicate a relative hydrate acidity of $Zn^{2+} > Fe^{2+} > Mn^{2+} > Mg^{2+} > Ca^{2+} > Na^{+} > K^{+}$ (Baes and Mesmer 1976; Stumm and Morgan 1996; Mähler and Persson 2012; Jackson et al. 2015), where the most acidic hydrate $[Zn(H_2O)_6]^{2+}$ has, by definition, the largest relative abundance of potentially reactive oxyanion species in water near physiological pH (~7.4). All of these hydrates are more acidic than bulk water ($pK_a$ 15.7) (Baes and Mesmer 1976). The standard free energy for ionization of an uncoordinated water molecule ($H_2O \rightarrow OH^- + H^+$) is large and positive (382.8 kcal/mol); coordination in a hexahydrate of $Mg^{2+}$, $Mn^{2+}$, or $Zn^{2+}$ reduces the energy of ionization by more than half (Bock et al. 1999).

Cations constrain water molecules to specific geometries. Though the number of water ligands for a hydrated cation is not fixed, especially when considering the dynamics of water molecules in solution, crystallographic structures reveal dominant coordination numbers (Table 6.4.1). Coordination by water ligands compresses metal ions: hydration decreases the effective ionic radius of the cation progressively with each water molecule added, while metal-oxygen bond distances increase (Shannon 1976; Bock et al. 1999). The effective ionic radius of a hexahydrated cation is also related to spin state and cation identity. Comparison of ionic radii, assuming hexahydrate coordination and low spin, yields relative atomic sizes $Fe^{2+} < Mn^{2+} < Mg^{2+} \cong Zn^{2+} < Ca^{2+} \cong Na^{+} < K^{+}$ (Shannon 1976). The radius of a hexahydrated $Fe^{2+}$ ion is less than half the radius of a hexahydrated $K^{+}$ ion. With the exception of $Zn^{2+}$, the radii of cation hexahydrates mentioned here correlate inversely with hydrate acidity. The availability of d-orbital electrons in the transition metals ($Fe^{2+}$, $Mn^{2+}$, and $Zn^{2+}$) is known to affect hydrate pKa (Roychowdhury-Saha and Burke 2006).

**TABLE 6.4.1**
**Properties of a Subset of Biologically Relevant Hydrated Cations**

| Cation | Effective Ionic Radii (Å) in a Hexahydrate (Shannon 1976) | Common Hydrate Coordination (Baes and Mesmer 1976; Jackson et al. 2015) | Experimentally Derived $pK_a$ (Baes and Mesmer 1976; Jackson et al. 2015) |
|---|---|---|---|
| $Fe^{2+}$ | 0.61[a], 0.78[b] | $[Fe(H_2O)_6]^{2+}$ | 9.3–9.5 |
| $Mn^{2+}$ | 0.67[a], 0.83[b] | $[Mn(H_2O)_6]^{2+}$ | 10.6–11.0 |
| $Mg^{2+}$ | 0.72 | $[Mg(H_2O)_6]^{2+}$ | 11.2–11.4 |
| $Zn^{2+}$ | 0.74 | $[Zn(H_2O)_6]^{2+}$ | 9.0 |
| $Ca^{2+}$ | 1.00 | $[Ca(H_2O)_8]^{2+}$ | 12.7–12.9 |
| $Na^{+}$ | 1.02 | $[Na(H_2O)_{6\text{-}8}]^{+}$ | 14.2 |
| $K^{+}$ | 1.38 | $[K(H_2O)_{6\text{-}8}]^{+}$ | 14.5 |

[a] Low spin (estimate);
[b] High spin.

Water molecule dynamics are suppressed by cations. The lifetime of a water molecule in the first coordination shell of a cation is generally longest for ions with the greatest charge density (e.g., highly charged with small ionic radius) (Diebler et al. 1969). It may be expected, based on ionic radii alone, that the relative exchange rate for the cations of Table 6.4.1 is $Fe^{2+} < Mn^{2+} < Mg^{2+} \cong Zn^{2+} < Ca^{2+} \cong Na^{+} < K^{+}$. Exchange rates have been estimated experimentally as $Mg^{2+} < Fe^{2+} \cong Mn^{2+} < Zn^{2+} < Ca^{2+} \cong Na^{+} \cong K^{+}$ (Diebler et al. 1969), where rates within one order of magnitude are considered within the range of uncertainty. The rate of exchange of water from the first coordination shell of $K^{+}$ (on the order of ~$10^{9}$ waters per second) occurs four orders of magnitude faster than from the first shell of $Mg^{2+}$ (Diebler et al. 1969).

Ions affect water enthalpically and entropically. In pure water, intramolecular interactions are dominated by hydrogen bonds. Hydrogens and electron lone pairs on each water participate in hydrogen-bonding interactions with surrounding water molecules. The high electronegativity of the oxygen makes each water molecule a dipole, with partial negative and positive charges. The partially negative oxygen of a water dipole interacts electrostatically with adjacent cations. Conversely, the partially positive charge of the dipole (bearing two hydrogens) interacts electrostatically with anions. Ions organize first-shell water molecules, affecting surrounding water molecules. The geometric perturbation of waters around an ion in aqueous solution reflects the outcome of competition between the ion and surrounding water molecules (or between electrostatic and hydrogen-bonding interactions) for the ion-constrained water. Theoretical studies suggest that the outcome of this competition strongly favors electrostatic interactions when a cation is small and densely charged, which disrupts canonical water-water hydrogen bonds (Hribar et al. 2002). Large, less-charge-dense cations have a greater tendency to share their most proximal water molecules with other water molecules and even promote canonical hydrogen bonding among surrounding waters (Hribar et al. 2002). The combined result is a difference in the distance of propagation of ion-induced organization of water. One report suggests that small, charge-dense cations reorganize up to two layers of water molecules around the ion (<5 Å), whereas large, less-charge-dense cations perturb only one layer (Collins et al. 2007). Differences in the organization of water around ions may explain, if only in part, the lack of interchangeability of ions in some biochemical processes.

### 6.4.2.2 Dehydration by Phosphate Oxyanions

Biology employs partially hydrated cations that constrain ligands other than water in the first coordination shell. Ligand binding to hexahydrated $Mg^{2+}$, for example, displaces a water molecule in the reaction (Mayaan et al. 2004):

$$L^{-q} + \left[Mg\left(H_2O\right)_6\right]^{2+} \rightarrow \left[Mg\left(H_2O\right)_5(L)\right]^{2-q} + H_2O \quad (6.4.1)$$

Single substitution of a water molecule for an alternate first-shell ligand type alters the structure of the $Mg^{2+}$ hydrate (Mayaan et al. 2004). If the ligand (L) is the oxyanion $OH^{-}$, for example, the interatomic distance between $Mg^{2+}$ and the oxygen atom of L is slightly less than the distance between $Mg^{2+}$ and each of its remaining five waters oxygens in $[Mg(H_2O)_5(OH)]^{+}$. In addition, the interatomic distance between $Mg^{2+}$ and the remaining five water oxygens increases slightly relative to $[Mg(H_2O)_6]^{2+}$. That is, the oxyanion ligand $OH^{-}$ is held more tightly by $Mg^{2+}$ than the neutral waters in $[Mg(H_2O)_5(OH)]^{+}$, and the neutral waters are less constrained (and possibly less acidic) than those in hexahydrated $Mg^{2+}$ (Figure 6.4.1).

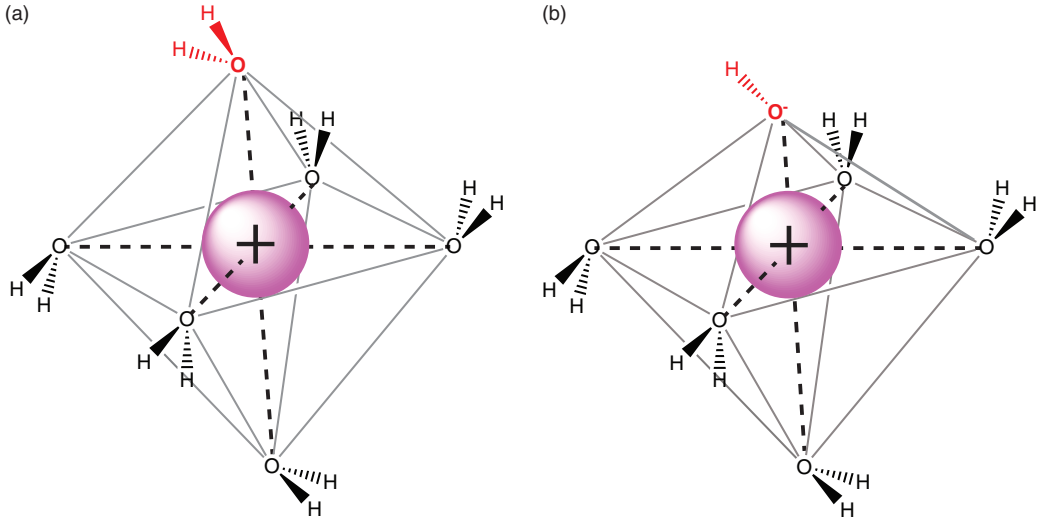


**FIGURE 6.4.1** Small oxyanion ligands of cations are held more tightly than neutral water. A conceptual model of the difference in interatomic distances between a charge-dense cation and a water ligand or oxyanion ligand. (a) A hexahydrated cation with octahedral coordination geometry and six roughly equal cation-water oxygen interatomic distances. (b) The interatomic distance between the cation and an oxyanion ligand, in this case $OH^{-}$, is less than remaining cation-water distances. The magenta sphere is a generic charge-dense cation. Neutral water ligand and oxyanion ligand are shown in red font. Remaining cation-water distances are increased slightly in panel B, relative to panel A. The change in bond length is exaggerated for clarity.

Phosphates and phosphate esters are common first-shell ligands of cations in biology. Like water, they are oriented, polarized, and constrained by cations. Most biological phosphate is covalently bound in adenosine mono-, di-, or tri- phosphate (AMP, ADP, or ATP); deoxyribonucleic acid (DNA); or ribonucleic acid (RNA) (Figure 6.4.2), and these molecules are well-documented partners of cations, especially $Mg^{2+}$. The transition states in condensation of the nucleic acid phosphodiester backbone by polymerases, ligases, and ribozymes, for example, are directly stabilized by divalent cations (Lykke-Andersen and Christiansen 1998; Steitz 1999; Doherty and Dafforn 2000; Lee et al. 2000; Yin and Steitz 2004; Ellenberger and Tomkinson 2008; Butcher 2011; Johnson-Buck et al. 2011).

Computation suggests that $Mg^{2+}$ binds phosphate or phosphate esters more tightly than water molecules. In work by

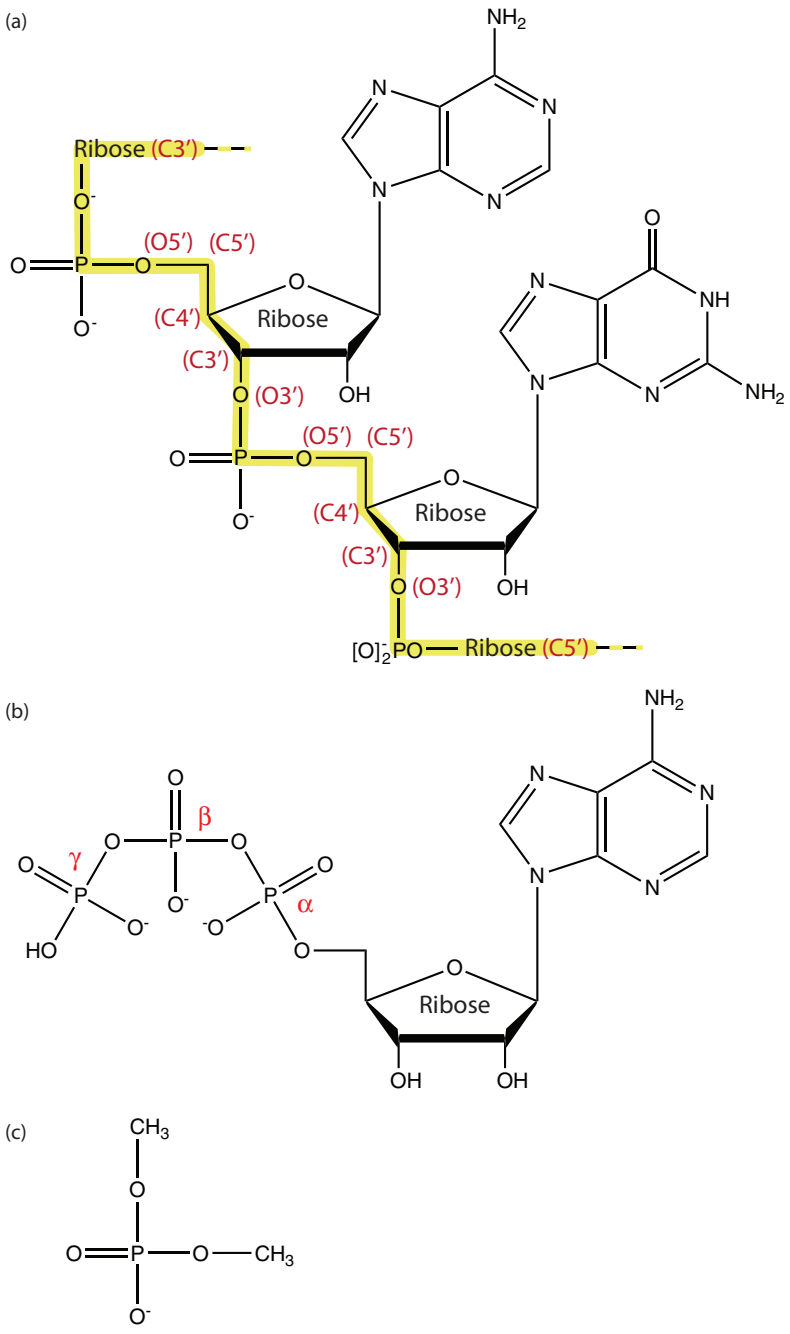


**FIGURE 6.4.2** Common biological ligands of cations. (a) Two monomers of RNA connected by the phosphodiester backbone (yellow highlight), with conventional ribose atom designations in parentheses. (b) Adenosine triphosphate (ATP) with conventional phosphate designations. (c) Dimethyl phosphate. Dimethyl phosphate, as discussed, is a molecular model representing the phosphodiester connecting unit of the nucleic acid backbone. Hydrogens on the ribose sugars of panels (a) and (b) have been omitted for clarity.

Mayaan et al. (2004), substitution of a single water molecule in $Mg^{2+}$ hexahydrate for a biologically derived ligand resulted in ligand-dependent changes in $Mg^{2+}$-ligand interatomic distances and remaining cation-water interatomic distances, consistent with Figure 6.4.1. $Mg^{2+}$ coordinated all evaluated small oxygen- and phosphate-bearing ligands with shorter cation-ligand oxygen interatomic distances than cation-water oxygen interatomic distances in single-substitution reactions (Mayaan et al. 2004). These ligands included free phosphate species hydrogen phosphate ($HPO_4^{2-}$) and dihydrogen phosphate ($H_2PO_4^-$), which dominate at physiological pH of 7.4, and dimethyl phosphate. Since the electronic structure of dihydrogen phosphate is somewhat different than phosphodiester, the dimethyl-phosphate anion ($CH_3—O—PO_2—O—CH_3)^-$ (Figure 6.4.2) is often used as a model system representing the phosphodiester connection between the base-bearing sugars of nucleic acids. In dimethyl phosphate, one methyl group is an analogue for the 3′ ribose carbon and the other an analogue for the 5′ carbon of the adjacent ribose sugar. Reported relative coordination distances for $Mg^{2+}$ are OH- < dimethyl phosphate < free phosphate species < water (Mayaan et al. 2004). In other words, $Mg^{2+}$ binds to dimethyl phosphate more tightly than to free phosphate or water.

The geometry of the nucleic acid backbone is cation-dependent. Work by Panteva et al. aiming, in part, to computationally replicate experimentally derived thermodynamic parameters for the interactions of $Mg^{2+}$, $Mn^{2+}$, or $Zn^{2+}$ with RNA, derived parameters for interactions of these cations with the nucleic acid analogue dimethyl phosphate. Their results suggest that contact and minimum energy distances between cation and phosphate follow a trend in which dimethyl phosphate oxyanion-$Mg^{2+}$ and -$Zn^{2+}$ distances are approximately equal and less than that of $Mn^{2+}$ (Panteva et al. 2015), suggesting that dimethyl phosphate binds more tightly to $Mg^{2+}$ and $Zn^{2+}$ than to $Mn^{2+}$. Fujimoto et al. (1994) reported cation-dependent variations in the nucleic acid hydrodynamic radius, in which $Na^+$ slightly decreased while divalent cations $Mg^{2+}$ and $Mn^{2+}$ substantially increased the hydrodynamic radius of DNA. These observations suggest cation-specific structural changes in nucleic acids, perhaps phosphodiester bond stabilization and/or changes in hydration.

$Mg^{2+}$ polarizes first-shell phosphate ligands, shortening phosphodiester bonds and leaving phosphorus more susceptible to nucleophilic attack. Upon substitution of a $Mg^{2+}$-constrained first-shell water with dimethyl phosphate in computational analyses, Mayaan et al. (2004) observed corresponding changes in the phosphate ligand. While the interatomic bond distance between phosphorus and the phosphate oxygen interacting with $Mg^{2+}$ increased, bond distances between the phosphorus atom and phosphate oxygens covalently bound to the methyl groups decreased, suggesting that $Mg^{2+}$ polarizes phosphate, drawing negative charge away from phosphate oxygens not directly coordinated by the cation. The magnitude of decrease in the length of the phosphodiester bonds of dimethyl phosphate has been calculated to be cation-specific, where the change induced by $Ni^{2+} > Mg^{2+} > Na^+$ (Zhang et al. 2015). Application of this observation to nucleic acids suggests that first-shell coordination of a backbone phosphate with cations may increase the reactivity of phosphorus while rigidifying the backbone by shortening the phosphodiester bonds in a cation-dependent manner. The expected change in bond lengths based on these calculations are within the range of precision of most nucleic acid structures but are believed to be corroborated by a few very-high-resolution structures.

## 6.4.3 CATIONS AS RNA LIGANDS

### 6.4.3.1 Conceptual Frameworks for Binding

Cations stabilize RNA through a continuum of associations, not just first-shell interactions. Williams and co-workers classified cation interactions with RNA as chelated, condensed, glassy, or diffuse, based on six criteria: relative population, number of first-shell RNA ligands, extent of mobility, dimensionality of mobility, contribution to RNA thermodynamic stability, and contribution to non-canonical RNA structure (Bowman et al. 2012).

The most populous ions in solutions of RNA are diffuse ions, which are fully hydrated without first-shell or first-shell water interactions with RNA and are no more restricted in mobility than bulk water. Diffuse cations are much more abundant than partially hydrated cations that directly coordinate RNA. The phosphodiester backbone of RNA is negatively charged and therefore self-repellant; diffuse cations electrostatically neutralize the RNA backbone. They interact with RNA by numerous weak, long-range electrostatic interactions (Manning 1969), contributing to the overall thermodynamic stability of nucleic acids and their complexes. These ions are undetectable in crystallographic structures in part due to their positional disorder. Diffuse ions do not stabilize specific non-canonical RNA structures.

Condensed ions (Manning 1969) have slightly attenuated mobility due to electrostatic or hydrogen-bonding interactions of one or more ion-coordinated waters with RNA or an RNA ligand. Their relative population and rate and dimensionality of diffusion are less than that of diffuse ions but are greater than glassy ions. Condensed ions neutralize charge that is more localized to the RNA than diffuse ions. Their population is sensitive to a local base pairing of nucleic acids and affects the geometry and conformational dynamics of the nucleic acid grooves (Lavery and Pullman 1981). Condensed ions can be visualized as a shell or coating on the surface of a three-dimensional RNA, extending beyond the van der Waals radius of the RNA.

Glassy cations have at least one first-shell RNA ligand and restricted mobility. They are typically found in the interior of the RNA, encased within the external three-dimensional surface of the native structure, such that the dimensionality of diffusion is reduced. The mobility of glassy cations is less than that of condensed cations. Glassy cations may contribute to stabilization of specific RNA structural states that are inaccessible in their absence. Divalent ions, especially $Mg^{2+}$, play a special role in the stability of RNA, due to their ability

to mediate strong tertiary interactions. Charge-dense $Mg^{2+}$ is glassy, with one first-shell RNA ligand, while less-charge-dense cations such as $Na^+$ and $K^+$ require four to five first-shell RNA ligands to similarly restrict diffusion.

Chelated cations, bearing more than one first-shell RNA ligand in the case of $Mg^{2+}$, are the least frequent ions in RNA structures but often have the most significance for the structure-function relationship. Chelated cations are typically at the interior of the three-dimensional surface of the native RNA. Their rate of diffusion is dependent on the number of first-shell RNA ligands. These cations are the least mobile of the four classes and, being rigidly bound by the RNA, are difficult to remove *in vitro* without disturbing the RNA structure.

The mode of $Mg^{2+}$-RNA interaction is influenced by local RNA structure. Experimental work suggests that sites of $Mg^{2+}$ chelation in RNAs are not random. Linear RNAs are less likely than folded RNAs to form first-shell interactions with $Mg^{2+}$, suggesting secondary structure and even sequence dependence (Porschke 1979). However, $Mg^{2+}$ forms first-shell interactions less readily with double-stranded RNA than with compact single-stranded RNA (Kankia 2003, 2004). In many cases, site-specific $Mg^{2+}$ binding and RNA conformation are interdependent: the conformational space in which an RNA achieves its native structure, including chelation of $Mg^{2+}$, is not available without $Mg^{2+}$, even with high concentration of monovalent cations (Draper et al. 2005; Grilley et al. 2006).

### 6.4.3.2 A Quantum Mechanical Perspective on First-Shell RNA-Cation Interactions

First-shell RNA-$Mg^{2+}$ complexes occur so frequently in ribosome and ribozyme x-ray structures that they appear to be fundamental units of RNA folding (Petrov et al. 2011). These complexes often appear in a singular and defined geometry, referred to here as the bidentate chelation complex (or bidentate clamp, Figure 6.4.3). Bidentate clamps are characterized by a 10-membered ring system ($Mg^{2+}$–$O^-$–P–O5′–C5′–C4′–C3′–O3′–P–$O^-$), which includes a single $Mg^{2+}$ chelated by phosphates of adjacent nucleotides (Hsiao et al. 2008; Hsiao and Williams 2009). Tri- and tetra-dentate RNA-$Mg^{2+}$ chelates have been noted (Hsiao et al. 2008).

Petrov et al. (2011) characterized the energetics of bidentate RNA-$Mg^{2+}$ clamps computationally using density functional theory (DFT). This work explains a special role of magnesium ions in the formation of tertiary interactions with RNA due to magnesium's enhanced binding ability with phosphodiester linkages and nucleobases. The $Mg^{2+}$-RNA interactions are amplified quantum effects of polarization and charge transfer due to high charge to radius ratio, which is the highest of all alkali and alkali-earth cations, making magnesium a unique ion in this group.

Bidentate chelation refers to cation association with two anions of the same ligand (in this case, the oxyanions of RNA phosphates) in the first coordination shell of the cation. The defined geometry and high stability of RNA-$Mg^{2+}$ bidentate clamps have been attributed to the tightly packed octahedral structure of the $Mg^{2+}$ first coordination shell (Brown 1992; Bock et al. 1999) and to the resulting non-canonical RNA backbone confirmation (Klein et al. 2004; Hsiao et al. 2008; Hsiao and Williams 2009). Using DFT, Petrov et al. explored the reaction:

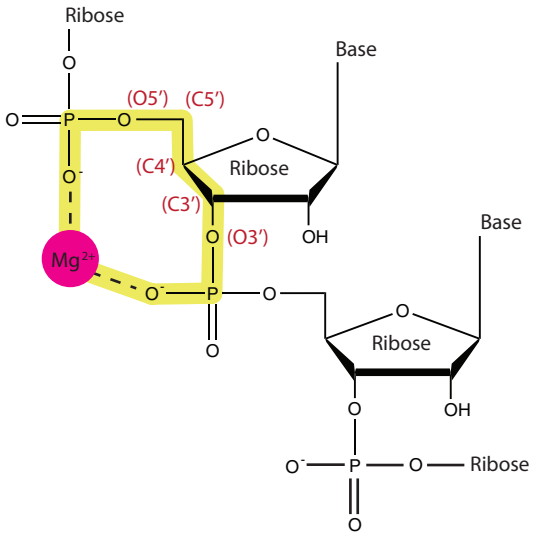


**FIGURE 6.4.3** The bidentate clamp characterized by a 10-membered ring system ($Mg^{2+}$–$O^-$–P–O5′–C5′–C4′–C3′–O3′–P–$O^-$), which includes a single $Mg^{2+}$ chelated by phosphates of adjacent nucleotides. (From Petrov et al. 2011; Hsiao, C. et al., Complexes of nucleic acids with group I and II cations, in *Nucleic Acid Metal Ion Interactions*, edited by N. Hud, pp. 1–35, The Royal Society of Chemistry, London, UK, 2008; Hsiao, C. and Williams, L.D., *Nucleic Acids Res.*, 37, 3134–3142, 2009.)

$$RNA^{2-} + \left[Mg\left(H_2O\right)_6\right]^{2+} \rightarrow \left[RNA\text{-}Mg\left(H_2O\right)_4\right]_{complex} + 2H_2O \quad (6.4.2)$$

In this reaction, two waters of hexahydrated magnesium are displaced as the cation is chelated by phosphate oxyanions on consecutive RNA nucleotides. Petrov et al. modeled the reaction by computationally optimizing the RNA structure in the absence and presence of $[Mg(H_2O)_6]^{2+}$, followed by optimization of the bidentate RNA-$Mg(H_2O)_4$ complex. Optimization was repeated with $[Na(H_2O)_6]^+$ or $[Ca(H_2O)_6]^{2+}$ in place of the $Mg^{2+}$ hexahydrate, with the objective of understanding the uniqueness of the role of $Mg^{2+}$ in complex stability.

RNA forms a more stable bidentate chelation complex with $Mg^{2+}$ than with $Na^+$ or $Ca^{2+}$ (Petrov et al. 2011). The RNA-$Mg(H_2O)_4$ complex is ~10 kcal/mol more stable than the RNA-$Ca(H_2O)_4$ complex. The $[RNA\text{-}Na(H_2O)_4]^-$ complex approaches neutral interaction energy and is unstable. The ionic radius of hexahydrated $Mg^{2+} < Ca^{2+} < Na^+$, therefore $Mg^{2+}$ forces first-shell oxyanion RNA ligands closer together than $Ca^{2+}$ or $Na^+$. The close proximity of the RNA oxyanions coordinated by $Mg^{2+}$ incurs an electrostatic penalty of ~10 kcal/mol from the opposing negative charges on the two oxygens; this is mitigated by other favorable energy components.

The octahedral coordination geometry of hexahydrate metals is distorted by RNA phosphate oxyanion ligands.

Distances from metal to oxygen are smaller for RNA phosphates than for water in $Mg^{2+}$ and $Ca^{2+}$ RNA chelation complexes. The metal-to-RNA phosphate oxyanion interatomic distances in the $Na^+$ RNA chelation complex are polymorphic. Optimization with $Na^+$ yields a monodentate structure with only one RNA phosphate oxyanion ligand in the first coordination shell of $Na^+$.

Energies of binding are substantial for small, charge-dense $Mg^{2+}$ complexes but are less so for $Ca^{2+}$ due to its larger size and for $Na^+$ due to its smaller charge. Decomposition of the interaction energy of bidentate clamps reveals that, for all cations modeled, electrostatic components make the greatest contributions to complex stability, followed by polarization (of the RNA phosphates) and charge transfer. There is a ~20 kcal/mol difference in the electrostatic contribution to bidentate clamp stability by $Mg^{2+}$ compared with $Ca^{2+}$; and a ~220 kcal/mol difference by $Na^+$ compared with $Mg^{2+}$. The polarization component is less than half of the electrostatic contribution for all cations. Charge transfer components include a net reduction of positive charge on each cation ($Mg^{2+}$: 0.2 $e^-$ > $Ca^{2+}$: 0.1 $e^-$ > $Na^+$: 0.1 $e^-$) (Petrov et al. 2011).

Magnesium's high charge density brings phosphate oxyanions of adjacent RNA nucleotides into closer proximity than $Ca^{2+}$ or $Na^+$, inducing non-canonical RNA backbone conformations found especially in catalytic RNAs. Complex formation may be driven, in part, by magnesium's preference for RNA's negatively charged and polarizable phosphate oxyanions over water. Though electrostatic energy components dominate stability, polarization and charge transfer components are not negligible. The small size of $Mg^{2+}$ creates a symmetrical distortion of the metal's octahedral coordination geometry, in which phosphate oxyanions are bound more tightly than water oxygens.

## 6.4.4 STRUCTURAL ROLES IN THE RIBOSOME

### 6.4.4.1 A $Mg^{2+}$ Scaffold for the Ribosome Peptidyl Transferase Center

All proteins of living organisms are synthesized by the ribosome, a highly conserved and ancient RNA-protein enzyme. The ribosome is the site of execution of the genetic code. With the help of aminoacyl tRNA synthetases and transfer RNAs, messenger RNA is decoded at the small subunit (SSU), while peptide bonds are made in the ribosomal LSU at the catalytic center, the peptidyl transferase center (PTC). The bacterial LSU contains two ribosomal RNA (rRNA) polymers, the 23S rRNA and the 5S rRNA, as well as numerous ribosomal proteins. The LSU rRNA of *Thermus thermophilus* is made up of more than 2,900 nucleotides, subdivided into seven domains (Domains 0, I, II, III, IV, V, and VI; Figure 6.4.4), based on the native structure common to all ribosomes (Petrov et al. 2014). Bokov, Steitz, Williams, and others observed that the occurrence of $Mg^{2+}$ in the LSU is greatest in Domain V near the PTC (Hansen et al. 2001; Klein et al. 2004; Bokov and Steinberg 2009; Hsiao et al. 2009).

Hsiao and Williams (2009) reported a framework of highly conserved $Mg^{2+}$ microclusters in the LSU. These microclusters include the 10-membered $Mg^{2+}$-RNA ring structure (Figure 6.4.3), modeled using DFT by Petrov et al. (2011), but in microclusters, the $Mg^{2+}$ ion is one of a pair of $Mg^{2+}$ ions chelated by a common bridging phosphate. The bridging phosphate, which has the form $Mg^{2+}_a$–$O^-$–P–$O^-$–$Mg^{2+}_b$, is part of the 10-membered chelation ring ($Mg^{2+}_a$–$O^-$–P–O5′–C5′–C4′–C3′–O3′–P–$O^-$–) (Hsiao and Williams 2009). As in Petrov et al. (2011), the phosphates of the chelation ring are contributed by adjacent nucleotides, but in a microcluster, at least one additional phosphate oxyanion interacts with at least one of the $Mg^{2+}$ ions.

$Mg^{2+}$-RNA microclusters support long-range intra- and inter-domain interactions relevant to the global structure of the ribosome. Hsiao and Williams (2009) found three ancient $Mg^{2+}$-RNA microclusters supporting the PTC and a fourth located near the LSU exit tunnel (Figure 6.4.4). These microclusters are conserved among archaea (represented by *Haloarcula marismortui*), bacteria (represented by *T. thermophilus*), eukarya, and mitochondria. Two of the ancient microclusters make intra-domain nucleotide connections, while the other two connect very remote rRNA nucleotides of multiple domains of the LSU. References to specific nucleotides are given as *T. thermophilus* residues in the *Escherichia coli* numbering convention.

Microcluster D2 connects Domain V of the LSU, near the PTC, to Domain II of the LSU (Figure 6.4.5). Here, the 10-membered ring is made of up of the phosphate groups and ribose atoms of A783 and A784 in Domain II. One $Mg^{2+}$ of this microcluster interconnects these nucleotides to the phosphate of A2589 in Domain V near the PTC. The other $Mg^{2+}$ links the phosphate of A784 to the phosphate of G2588. Five phosphate oxygens of four nucleotides representing two disparate locations in the rRNA sequence are bridged by these two $Mg^{2+}$.

Microcluster D4 connects Domain IV of the LSU to Domain II (Figure 6.4.6). There are two 10-membered rings in this microcluster. One ring is made up of the phosphate groups and ribose atoms of C1782 and A1783; the other is made up of the phosphate groups and ribose atoms of A1783 and A1784. All of these nucleotides are in LSU Domain IV. The phosphate of A1780, a non-consecutive nucleotide of Domain IV, chelates one of these $Mg^{2+}$. One $Mg^{2+}$ of this microcluster is also chelated by the phosphate of U740 in Domain II.

Microclusters D1 and D3 make long-range intra-domain connections of the rRNA (Figure 6.4.4). Microcluster D1 links RNA nucleotides of Domain V that are not adjacent in the linear sequence or secondary structure; microcluster D3 links non-adjacent nucleotides of Domain III. In microcluster D1, the 10-membered ring is made of up of the phosphate groups and ribose atoms of C2498 and C2499. The phosphate of A2448 (50 nucleotides away in the primary sequence) bridges both of the microcluster magnesiums. In microcluster D3, located near the exit tunnel, the 10-membered ring is made of up of the phosphate groups and ribose atoms of

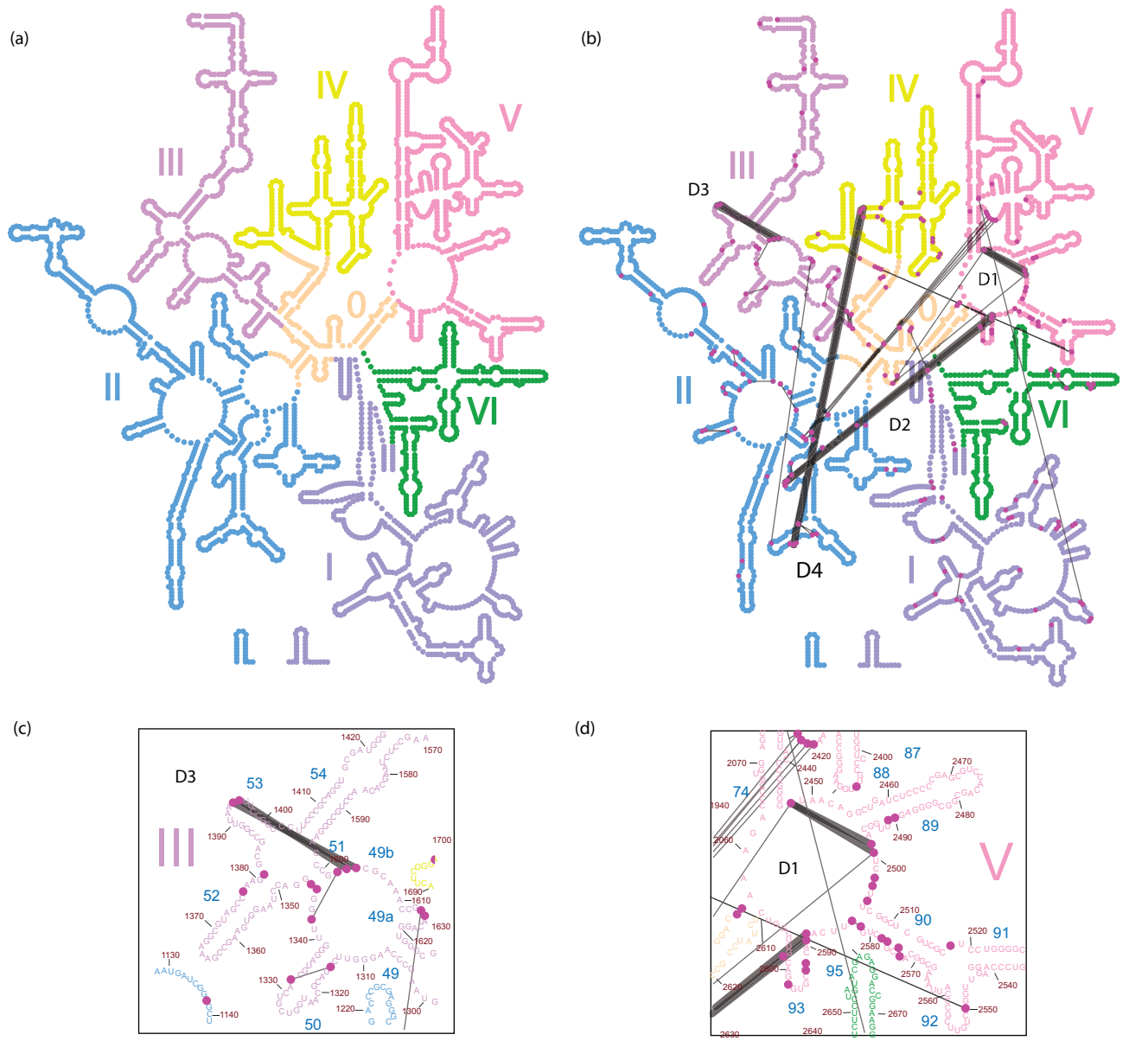


**FIGURE 6.4.4** Ancient $Mg^{2+}$ microclusters interconnect domains of 23S rRNA in the LSU. (a) Divisions in rRNA secondary structure Domains 0, I, II, III, IV, V, and VI are represented by changes in nucleotide color. (b) Microclusters D1, D2, D3, and D4 are shown as thick gray lines connecting nucleotide phosphates sharing a common first-shell $Mg^{2+}$. Other first-shell $Mg^{2+}$ interactions are shown as thin gray or black lines (some have been omitted for clarity). Nucleotides are colored spheres. $Mg^{2+}$ ions are magenta spheres. (c) $Mg^{2+}$ microcluster D3 of Domain III. (d) $Mg^{2+}$ microcluster D1 of Domain V. Secondary structure data generated with RiboVision (Bernier et al. 2014); microcluster data from Hsiao. (From Hsiao, C. and Williams, L.D., *Nucleic Acids Res.*, 37, 3134–3142, 2009.)

A1603, along with the phosphate group of C1604. Phosphates of U1394 and U1395 chelate the $Mg^{2+}$ of this microcluster.

$Mg^{2+}$ microclusters cause bases to unstack, priming them for short- and long-range rRNA interactions. Microcluster D2 unstacks base A784 of Domain II, which forms a pocket for ribosomal protein L2, and base A2587 of Domain V, which intercalates with unstacked bases C1782 and A1783 from microcluster D4 of Domain IV (Figure 6.4.5). Microcluster D4 induces a large array of unstacked bases in Domain IV, some of which intercalate with A2587 (unstacked in D2) of Domain V (Figure 6.4.6). Microcluster D1 unstacks G2447 from A2448 and A2497 from C2498 in Domain V. Microcluster D3 unstacks base U1602 from A1603 and base A1393 from U1394 in Domain III.

The $Mg^{2+}$-RNA microcluster appears to be an ancient motif, with roles in rRNA folding and function, though it does not participate directly in peptide bond formation. The microclusters and rRNA elements linked by microclusters are conserved over evolution among archaea, bacteria, eukarya, and mitochondrial rRNA. $Mg^{2+}$-RNA microclusters have been identified in other rRNAs, including the bacterial SSU rRNA (Wimberly et al. 2000), and the P4-P6 domain of the *Tetrahymena thermophila* Group I intron ribozyme (Cate et al. 1997).

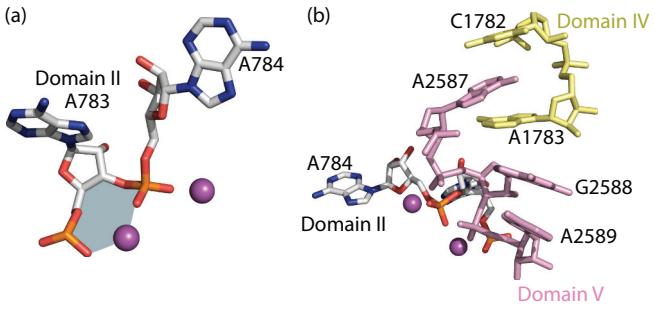


**FIGURE 6.4.5** Inter-domain $Mg^{2+}$-RNA microcluster D2 of 23S rRNA. (a) The D2 microcluster is a 10-membered ring (composed of a single $Mg^{2+}$, the phosphate and ribose backbone atoms of nucleotide A783, and the phosphate of A784) and a second $Mg^{2+}$ ion bridged by the common phosphate of A784. The area of the 10-membered ring is shown gray. RNA carbons are light gray, oxygens red, phosphorus orange, and nitrogen blue. Magnesium ions are magenta spheres. D2 microcluster nucleotides A783 and A784 are in Domain II of the 23S rRNA secondary structure. (b) The D2 microcluster mediates short- and long-range interactions in the 23S rRNA. The two $Mg^{2+}$ of D2 are chelated by nucleotide phosphates of Domain II (atoms colored as in panel [a]) and Domain V rRNA (pink). Microcluster formation induces a non-canonical RNA backbone conformation, unstacking A2587 of Domain V, which intercalates with C1782 and A1783 of Domain IV (yellow). Structure of *T. thermophilus* [PDB 2J01 (obsolete). Superseded by 4V51]; microcluster data from Hsiao. (From Hsiao, C. and Williams, L.D., *Nucleic Acids Res.*, 37, 3134–3142, 2009.)

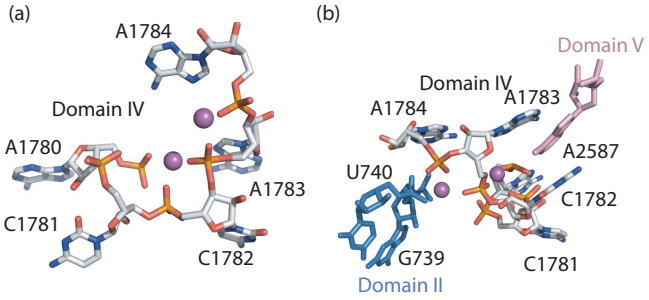


**FIGURE 6.4.6** Inter-domain $Mg^{2+}$-RNA microcluster D4 of 23S rRNA. (a) The D4 microcluster has two consecutive 10-membered rings composed of two $Mg^{2+}$ and the phosphate and ribose backbone atoms of nucleotides C1782 and A1783, and A1783 and A1784. The phosphate of A1780 also chelates one of the $Mg^{2+}$. (b) The D4 microcluster mediates short- and long-range interactions in the 23S rRNA. One $Mg^{2+}$ of D4 is chelated by the phosphate of U740 of Domain II (blue). C1782 and A1783 intercalate with A2587 of Domain V (pink). Structure of *T. thermophilus* [PDB 2J01 (obsolete). Superseded by 4V51]; microcluster data from Hsiao. (From Hsiao, C. and Williams, L.D., *Nucleic Acids Res.*, 37, 3134–3142, 2009.)

### 6.4.4.2 Ribosomal RNA Folding in the Absence of Proteins

The 23S rRNA of the ribosome LSU is a single polymer, thousands of nucleotides in length. Folding of the native ribosome to its catalytic state *in vivo* occurs with cations, including $Mg^{2+}$; many ribosomal proteins; and post-transcriptional modifications.

It has been shown that the 23S rRNA, without ribosomal proteins or post-transcriptional modifications, can fold to form RNA-RNA interactions resembling those of the native ribosome (Lenz et al. 2017). Lenz et al. used a chemical footprinting technique called Selective 2′ Hydroxyl Acylation Analyzed by Primer Extension (SHAPE) (Mortimer and Weeks 2007) to assess the reactivity of each ribose 2′-OH in the 23S rRNA sequence to an electrophile. SHAPE reactivity can be viewed as a measure of a nucleotide's mobility or tendency to adopt a reactive conformation, meaning that the least-reactive nucleotides are the most likely participants in canonical hydrogen-bonding interactions.

Lenz et al. (2017) found that $Na^+$ alone supports formation of native-like rRNA secondary structure in the 23S rRNA. In other words, regions of rRNA such as helices, which are base-paired in the x-ray crystallographic structure, show minimal reactivity by SHAPE, whereas bases in or near the bulges and loops of rRNA, which should be more mobile and/or unpaired, are reactive.

Structural collapse of 23S rRNA to form the tertiary interactions of the native ribosome LSU requires $Mg^{2+}$ (Lenz et al. 2017). Addition of $Mg^{2+}$ alters the pattern of reactivity, observed with $Na^+$ alone. Some bases or regions of bases at or near bulges and loops become more, and others less, reactive in the presence of $Mg^{2+}$ and $Na^+$ than in the presence of $Na^+$ alone. The reactivities in helical regions, unreactive in the presence of $Na^+$ alone, are largely unaltered in the presence of $Mg^{2+}$. However, non-helical regions showed changes in reactivity upon addition of $Mg^{2+}$. Inspection of regions of crystallographic structures of native ribosomes showing altered reactivity by SHAPE suggests that these regions are largely associated with or are proximal to (1) known RNA-RNA tertiary interactions or (2) known RNA-protein interactions. Regions of altered reactivity are not limited to nucleotides expected to form first-shell tertiary interactions with $Mg^{2+}$, as observed by Hsiao and Williams (2009).

Magnesium-induced tertiary interactions include formation of an intricate inter-domain rRNA interaction network. Nucleotides within secondary structure domains come into close proximity in three-dimensional space on folding and formation of the native 23S rRNA structure, interacting, in part, via base-pairing, base stacking, and phosphate-$Mg^{2+}$ interactions. Of the 21 possible combinations of domain-to-domain interactions, the native 23S rRNA (as represented by bacterium *T. thermophilus*) has 14 interactions. Lenz et al. (2017) found that 12 of the 14 domain-domain interactions are detectable as $Mg^{2+}$-induced by SHAPE in the absence of ribosomal proteins. Here, one domain-domain interaction may be represented by a series of nucleotide-nucleotide or nucleotide-$Mg^{2+}$ interactions.

$Mg^{2+}$ appears necessary to position rRNA nucleotides for native interactions with ribosomal proteins and form a catalytic structure. Folding of the LSU 23S rRNA in the presence of $Mg^{2+}$ induces a native-like structure in which the rRNA has collapsed to form much of the essential inter-domain architecture.

### 6.4.4.3 Ribosomal RNA Folding in the Presence of Proteins

Divalent cation-rRNA backbone interactions induce conformational changes that accommodate other ligands. Magnesium-microcluster D2 forms a pocket in the ribosome for ribosomal protein L2 (now known as uL2; Ban et al. 2014). Hsiao et al. found that $Mg^{2+}$-microcluster D2 connects Domain V of the 23S rRNA, near the PTC, to Domain II of the 23S rRNA (Hsiao and Williams 2009). The 10-membered ring of this microcluster is made of up A783 and A784 in Domain II. One $Mg^{2+}$ forms a phosphate-mediated tertiary interaction with A2589 in Domain V near the PTC. The other $Mg^{2+}$ forms a phosphate-mediated tertiary interaction with G2588 of Domain V. The D2 microcluster unstacks base A784 of Domain II, forming a pocket for ribosomal protein uL2 (Figure 6.4.5).

Ribosomal protein uL2 is unique in that its interaction with 23S rRNA appears to be more extensively mediated by $Mg^{2+}$ than the interactions of other LSU proteins. The two $Mg^{2+}$ ions of the D2 microcluster have (in sum) 12 first-shell ligands: five RNA phosphate oxyanions and seven waters (Petrov et al. 2012). Protein uL2 interacts directly with four of these waters through two highly conserved amino acids, alanine (or valine) and asparagine, interposed by a conserved methionine. The conserved uL2 sequence is most frequently alanine-methionine-asparagine (AMN) (Petrov et al. 2012). In *T. thermophilus,* these are residues Ala225, Met226, and Asn227 (Figure 6.4.7).

The observed interaction at the D2 microcluster is protein-water-$Mg^{2+}$-RNA, where the protein-water components interact via hydrogen bonds between a protein carbonyl and an acidic $Mg^{2+}$-bound water. In addition to directly coordinating the phosphates of A783, G784, G2588 and A2589 of the D2 microcluster, the $Mg^{2+}$ ions, through their water ligands, interact with lone pairs of electrons on the backbone carbonyl of Ala225 and the side-chain carbonyl of Asn227 (Figure 6.4.7). Petrov et al. (2012) dissected and examined the stability of each component of the D2 microcluster protein-water-$Mg^{2+}$-RNA interaction by using quantum methods.

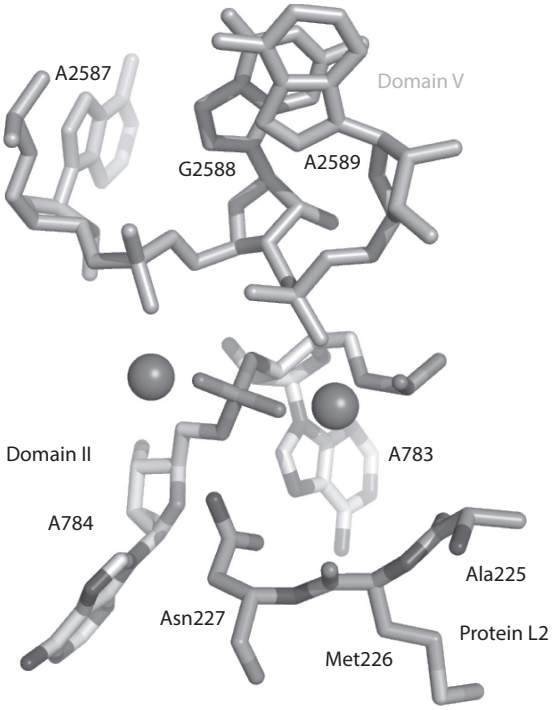


**FIGURE 6.4.7** The microcluster D2-ribosomal protein L2 interaction, an RNA-$Mg^{2+}$-water-protein interaction. Phosphates of A783, A784, G2588, and A2589 coordinate two $Mg^{2+}$ ions and form microcluster D2. These magnesium ions are also chelated by the backbone carbonyl of Ala225 and the side-chain carbonyl of Asn227. Structure of *T. thermophilus* [PDB 2J01 (obsolete). Superseded by 4V51] adapted from Petrov et al. (From Petrov, A.S. et al., *J. Phys. Chem. B*, 116, 8113–8120, 2012.)

In $Mg^{2+}$ microcluster D2, the $Mg^{2+}$ ions stabilize amino acid-water interactions, while the RNA ligands of the $Mg^{2+}$ attenuate them slightly. Though Ala225 and Asn227 each have favorable and roughly equal interaction energies with water alone, interaction energies with water bound to $Mg^{2+}$ in a hexahydrate (e.g., $[Mg(H_2O)_6]^{2+}$) are four-fold more favorable. The charge transfer component of the interaction energies implies that the charge on the amino acid carbonyl is transferred to the $Mg^{2+}$ by polarization of the mediating water. To understand the effect of the RNA phosphates on the stability of the complex, two dimethyl phosphate molecules (Figure 6.4.2) were used to simulate chelation of $[Mg(H_2O)_4]^{2+}$ by the RNA bidentate clamp. Chelation of the metal by the RNA analog decreases the overall stability of the amino acid-water-$Mg^{2+}$-RNA complex by roughly one third, though interaction energies remained favorable. In other words, chelation of the $Mg^{2+}$ by the phosphates of the RNA analog decreases polarization of the remaining water ligands of the $Mg^{2+}$ and thus the acidity of the protein-mediating water, slightly attenuating the strength of the water-protein interaction. Even so, the amino acid-water-$Mg^{2+}$-RNA complex remains more than two-fold more stable than the amino acid-water complex, and the charge transfer component of the interaction energy remains strong enough to

infer that some charge from the amino acid carbonyl remains with the $Mg^{2+}$.

The D2 microcluster stabilizes a segment of protein uL2 through orientation and polarization of water molecules. The AMN segment of protein uL2 interacts with the D2 microcluster through six hydrogen bonds. Four of these are with $Mg^{2+}$-polarized water molecules. The backbone carbonyl oxyanion of Ala225 hydrogen bonds (H-bonds) with two $Mg^{2+}$-bound waters of the same D2 $Mg^{2+}$ and one 2′OH of rRNA A782. The side-chain carbonyl of Asn227 H-bonds with one water of each D2 $Mg^{2+}$, while the side-chain amine of Asn227 shares a hydrogen with a phosphate oxyanion of A784. To determine the role of the $Mg^{2+}$ in supporting this interaction, Petrov et al. (2012) used DFT to examine the stability of the hydrated L2 segment, AMN-water, with and without the $Mg^{2+}$ and RNA of the D2 microcluster. The AMN-water-$Mg^{2+}$-RNA complex is four-fold more stable than AMN-water, even though AMN does not interact directly with the $Mg^{2+}$. In the case of uL2, neither $Mg^{2+}$ nor RNA alone stabilizes the interaction with ribosomal protein; it is rather the orientation and polarization of the water molecules by $Mg^{2+}$ that enhance stability.

## 6.4.5 RIBOZYME FUNCTION

### 6.4.5.1 Ribozymes with $Mg^{2+}$, $Fe^{2+}$, and Other Cations

Cations in the LSU play, to current knowledge, strictly structural roles in their support of the peptidyl transfer reaction. Although $Mg^{2+}$ is necessary for folding and function of the LSU, there is not a direct role for any $Mg^{2+}$ ion in the mechanism of peptidyl transferase (Noller et al. 1992). This is not the case for all catalytic RNAs.

The transition states of many ribozymes (see also Chapters 6.4 and 6.6) are directly stabilized by divalent metals (Butcher 2011; Johnson-Buck et al. 2011). In the activity of the *in vitro* evolved L1 ligase ribozyme (Robertson and Scott 2007), for example, the 5′ α-phosphate of a nucleotide triphosphate (Figure 6.4.2) is polarized by a $Mg^{2+}$ ion, priming the α-phosphorus for nucleophilic attack by an acidic 3′-OH of the adjacent nucleotide. Nucleophilic attack of the 3′-OH on the 5′ α-phosphate completes the phosphodiester bond necessary for backbone ligation, generating a pyrophosphate leaving group (Robertson and Scott 2007). In the hammerhead ribozyme, an acidic metal-coordinated water at the active site is believed to donate a hydrogen, stabilizing the oxyanion leaving group during cleavage (Scott et al. 1995; Murray et al. 1998; Scott 2007). Unlike the L1 ligase ribozyme, which requires the divalent metal for activity, the hammerhead ribozyme retains some activity in the absence of divalent metals in high (e.g., >1.0 M) $Na^+$ concentration (Nakano et al. 2014) or low $Na^+$ concentration (100 mM) at freezing temperature (Lie and Wartell 2015).

The hammerhead ribozyme, in particular, has a promiscuous relationship with cations. Computed barriers in the free-energy landscapes of "metal migration" within the active site of the self-cleaving hammerhead ribozyme are generally larger for $Mg^{2+}$ and $Zn^{2+}$ than for $Mn^{2+}$ (Panteva et al. 2015). This observation is consistent with experimental work showing that at pH 7, in the presence of 0.1 M NaCl, the catalytic rate of self-cleavage by the hammerhead is greater with $Mn^{2+}$ than with $Mg^{2+}$ (Hunsicker and DeRose 2000).

Compaction and formation of secondary structure in the Group I intron P4-P6 domain ribozyme of *T. thermophila* are supported by $Na^+$ alone, but divalent cations are needed to induce tertiary structure (Cate et al. 1997; Deras et al. 2000). Athavale et al. (2012) used SHAPE to probe the P4-P6 domain in the presence of $Na^+$ and observed low SHAPE reactivity, indicative of canonical base pairing, in regions observed in the crystallographic structure to be helical, while loop regions (unpaired in the structure) tended to be much more reactive. Addition of mM concentrations of $Mg^{2+}$ caused distinct changes in SHAPE reactivity, suggestive of specific magnesium binding and formation of tertiary RNA structure (Figure 6.4.8).

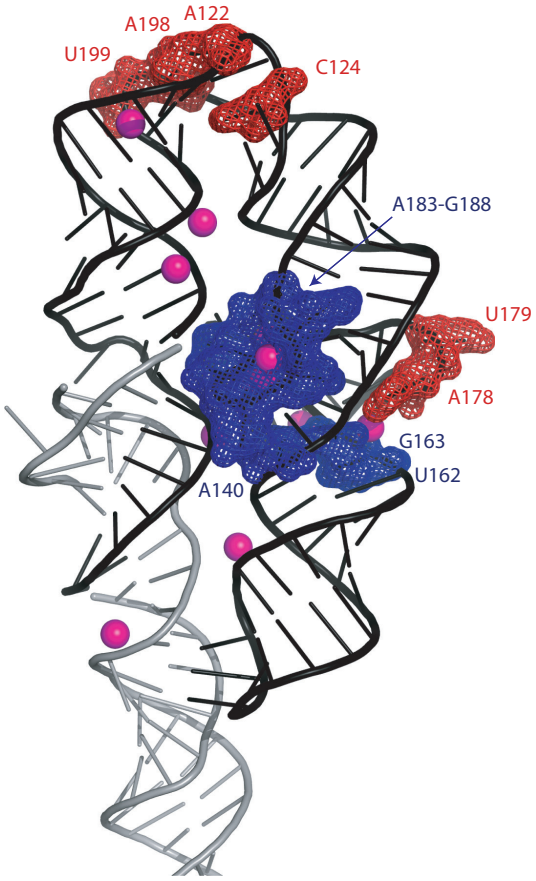


**FIGURE 6.4.8** SHAPE reactivity of the Group I intron P4-P6 domain ribozyme of *T. thermophila* is altered in the presence of $Mg^{2+}$ or $Fe^{2+}$. Sites of pronounced increases in SHAPE reactivity in the presence of $Mg^{2+}$ or $Fe^{2+}$ and $Na^+$ (compared with $Na^+$ alone) are red; decreases are blue. RNA for which there is moderate to no change in SHAPE reactivity with $Mg^{2+}$ or $Fe^{2+}$ is black. RNA for which SHAPE data are not available is shown in gray. $Mg^{2+}$ ions are magenta spheres. SHAPE data are adapted from Athavale et al. (2012), displayed on PDB 1GID (Cate et al. 1996). The structure was crystallized in the presence of $Co^{2+}$ (not shown), which was not present in SHAPE reactions by Athavale et al. (From Athavale, S.S. et al., *PLoS One*, 7, e38024, 2012.)

Most of the residues having an increase in SHAPE reactivity in the presence of $Mg^{2+}$ (compared with $Na^{+}$ alone) bear a C2′-endo sugar pucker in structure PDB 1GID (Cate et al. 1996). This geometry of the ribose, typical of DNA, but rare and restricted to non-helical regions of RNA structures (Auffinger and Westhof 1997), was previously demonstrated to have enhanced reactivity by SHAPE (Cate et al. 1996; Vicens et al. 2007). The region with a decrease in SHAPE reactivity in the presence $Mg^{2+}$ is consistent with packing of phosphates by $Mg^{2+}$ in a core inaccessible to solvent (Cate et al. 1997). $Mg^{2+}$ microclusters are present in this region of the P4-P6 RNA (Cate et al. 1997; Hsiao and Williams 2009).

$Fe^{2+}_{(aq)}$ oxidizes and precipitates rapidly in the presence of atmospheric oxygen, but under anoxic conditions, it induces folding of P4-P6 domain RNA to a near-native state. Athavale et al. (2012) demonstrated that the pattern of SHAPE reactivity in P4-P6 domain RNA in the presence of $Fe^{2+}$ under anoxic conditions closely resembles that in the presence of $Mg^{2+}$. Regions of RNA with pronounced increases in SHAPE reactivity upon the addition of $Mg^{2+}$ (compared with $Na^{+}$ alone) also increase in reactivity upon addition of $Fe^{2+}$. Parallel decreases in SHAPE reactivity were also observed in other regions of the RNA, suggesting that, in anoxia, $Fe^{2+}$ replaces $Mg^{2+}$, without perturbation of the native structure of the P4-P6 ribozyme.

Catalysis by the L1 ligase or hammerhead ribozyme occurs at an enhanced rate in the presence of $Fe^{2+}$. Athavale et al. (2012) compared the catalytic rate of the L1 ligase ribozyme in $Na^{+}$, $Na^{+}/Mg^{2+}$, and $Na^{+}/Fe^{2+}$. As expected, the L1 ligase was inactive in $Na^{+}$ alone. Micromolar concentrations of $Mg^{2+}$ or $Fe^{2+}$ induced catalytic activity. Surprisingly, the rate of $Fe^{2+}$-induced catalysis was 25 times that of $Mg^{2+}$-induced catalysis. A similar affect was observed for the hammerhead ribozyme: catalysis in the presence of $Fe^{2+}$ initiated at a rate three times higher than in the presence of $Mg^{2+}$. The interchangeability of $Mg^{2+}$ and $Fe^{2+}$ in RNA folding and function is supported by theoretical computational analyses that revealed only subtle differences in the coordination geometries of these RNA-divalent metal (RNA-$M^{2+}$) complexes. Furthermore, the calculations demonstrated that stability of RNA-$M^{2+}$ complexes is enhanced when $Mg^{2+}$ is replaced with $Fe^{2+}$ (Petrov et al. 2011; Athavale et al. 2012), possibly due to the availability of d-orbitals in $Fe^{2+}$.

## 6.5.6 CONCLUSIONS

Fundamental biochemical processes of life as we know it depend on inorganic cations. Inorganic cations in association with RNA are always hydrated to some extent, and the importance of water in their interactions cannot be overstated. The unique properties of each cation—principally size and charge—alter the mobility and physicochemical properties of first-shell waters, which in turn affect surrounding water and non-water molecules. The energetic penalties associated with cation dehydration are a part of the net energy of reaction for every first-shell interaction with a biological ligand.

Inorganic cations have a special relationship with the phosphodiester backbone of nucleic acids. Backbone phosphates are anionic and highly polarizable, coordinating some cations with more compact geometry than others. The intricacies of a cation's individual properties can be viewed as magnified by interactions with phosphate esters, due to phosphate's enhanced polarizability relative to water. Magnesium stabilizes RNA through a continuum of associations, from neutralization of bulk negative charge in solution by mobile hexahydrates to compact first-shell coordination of up to four RNA backbone phosphates, while the range of associations of $Na^{+}$ and other large, monovalent cations is less diverse (Bowman et al. 2012).

The role of inorganic cations in protein translation provides an essential perspective on their importance in biology and relevance to the origin of life. Multiple high-resolution crystal structures of the ribosome reveal that the core structure of the LSU is essentially unchanged throughout extant life, including the locations of cations and their binding sites' geometries (Hsiao and Williams 2009). When compared with other functional RNAs (ribozymes), the rRNA of the LSU is immense in length and complexity. An understanding of the principles underlying folding of such a large RNA to the universal conformation of peptide bond synthesis informs our understanding of LUCA and the constraints under which it might have evolved.

The LSU provides every indication that it has been dependent on $Mg^{2+}$ or $Mg^{2+}$-like divalent cations for folding and function since, and likely before, LUCA. Reoccurring motifs of rRNA in first-shell interactions with $Mg^{2+}$ help to organize the three-dimensional structure of the LSU, though $Mg^{2+}$ does not participate in catalysis directly. A recent study suggests that $Mg^{2+}$ may also play an indirect role in stabilization of pre- and post-peptidyl transfer states (Polikanov et al. 2014). For perspective, $Mg^{2+}$ ions observed in a crystal structure of the ribosome are shown in Figure 6.4.9.

These motifs include the bidentate RNA-$Mg^{2+}$ clamps and $Mg^{2+}$ microclusters (Hsiao and Williams 2009; Petrov et al. 2011). In an RNA-$Mg^{2+}$ clamp, the phosphates of two consecutive nucleotides chelate a single $Mg^{2+}$, altering the geometry of the metal hydrate and in turn the local properties of the RNA. Computation suggests that $Na^{+}$ is incapable of stabilizing this type of RNA geometry. In a $Mg^{2+}$ microcluster, one phosphate of an RNA-$Mg^{2+}$ clamp serves as a bridge to a second $Mg^{2+}$ ion, which, in three-dimensional structures, coordinates and restrains the phosphate of nucleotide(s) that are hundreds to more than a thousand nucleotides away in the primary sequence. $Mg^{2+}$ microclusters induce non-canonical geometries to RNA bases, priming them for interaction with nucleotides from other domains and ribosomal proteins. Twelve of the 14 interdomain interactions in the LSU 23S rRNA of *T. thermophilus* are $Mg^{2+}$-induced (Lenz et al. 2017).

The $Mg^{2+}$ dependencies of the LSU extend to interactions of first-shell waters with rRNA and ribosomal proteins. The first-shell waters of $Mg^{2+}$ also stabilize the LSU. In one case, waters coordinating the $Mg^{2+}$ of the D2 microcluster participate in hydrogen-bonding interactions with side-chain and backbone carbonyls of two highly conserved residues

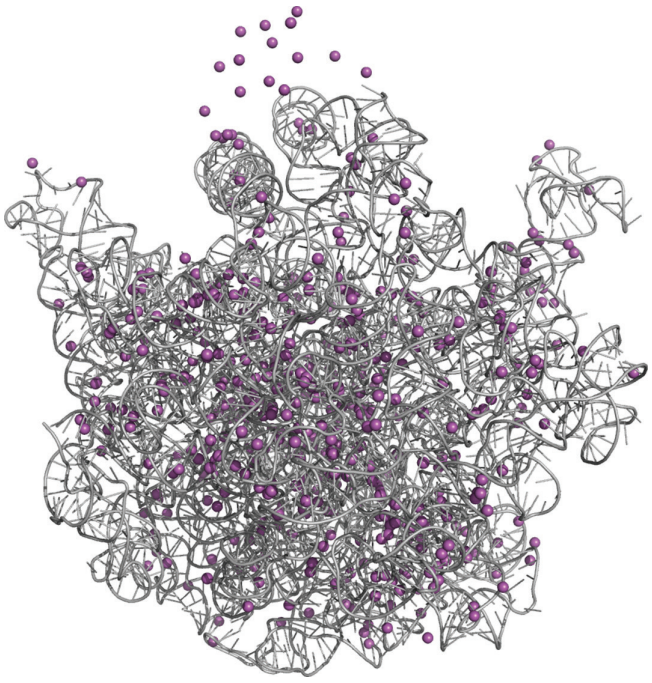

**FIGURE 6.4.9** Prevalence of $Mg^{2+}$ (magenta spheres) in the 23S rRNA crystal structure. Structure of *T. thermophilus* [PDB 2J01 (obsolete). Superseded by 4V51].

of ribosomal protein uL2 (Petrov et al. 2012). $Mg^{2+}$ substantially increases the favorability and stability of the uL2-water interactions through orientation and polarization of the water molecules.

The ribosome is our telescope to origins and evolution of life (Gutell et al. 1994). Evolution appears to have perpetuated inorganic ion-dependent mechanisms that are essential and somewhat resilient to ion substitution. Three of the four ribozymes discussed, the Group I Intron P4-P6 domain, the hammerhead, and the ribosome LSU, are natural ribozymes. The P4-P6 domain and hammerhead ribozymes accommodate a broader range of cations in function and folding than the *in vitro* selected L1 ligase (Hunsicker and DeRose 2000; Doudna and Cech 2002; Travers et al. 2007; Athavale et al. 2012), yet the most central ribozyme of life, the ribosome, has just recently been shown to catalyze peptidyl transferase with a cation other than $Mg^{2+}$ (Bray et al. submitted). $Fe^{2+}$, which has been largely insoluble and toxic to life in the absence of protein chaperones since the Great Oxidation Event, appears to be a capable and, in some cases, an even superior substitute for $Mg^{2+}$ in RNA folding and function.

Cation substitutions over evolution extend beyond nucleic acids. An almost-singular mechanism with transition states stabilized by divalent cations underpins a variety of nucleic-acid-processing proteins (Lykke-Andersen and Christiansen 1998; Steitz 1999; Doherty and Dafforn 2000; Lee et al. 2000; Yin and Steitz 2004; Ellenberger and Tomkinson 2008). As a group, but with species-specific exceptions, these enzymes generally tolerate partial to complete substitutions of $Mg^{2+}$ for $Mn^{2+}$ and occasionally other cations. One analysis ties the early evolution of eukaryotes to an oxic Earth and prokaryotes to an anoxic one, based on trends in metal substitutions in metallo-proteins (Dupont et al. 2006). Another result of this work is that the overall abundance of metallo-proteins was found to scale with proteome size, suggesting that biology's dependence on inorganic cations is not vestigial.

## ACKNOWLEDGMENTS

We thank Roger M. Wartell for critical review of an early version of the manuscript and Afrah Ghauri and Chieri Ito for careful editorial review. This work was supported by the National Aeronautics and Space Administration (NNX16AJ29G and NNX16AJ28G) and the National Science Foundation (1724274).

## REFERENCES

Aguirre, J. D., and V. C. Culotta. 2012. Battles with iron: Manganese in oxidative stress protection. *Journal of Biological Chemistry* 287 (17): 13541–13548. doi:10.1074/jbc.R111.312181.

Anjem, A., S. Varghese, and J. A. Imlay. 2009. Manganese import is a key element of the OxyR response to hydrogen peroxide in *Escherichia coli*. *Molecular Microbiology* 72 (4): 844–858. doi:10.1111/j.1365-2958.2009.06699.x.

Athavale, S. S., A. S. Petrov, C. Hsiao et al. 2012. RNA folding and catalysis mediated by iron (II). *PLoS One* 7 (5): e38024. doi:10.1371/journal.pone.0038024.

Auffinger, P., and E. Westhof. 1997. Rules governing the orientation of the 2′-hydroxyl group in RNA11.Edited by I. Tinoco. *Journal of Molecular Biology* 274 (1): 54–63. doi:10.1006/jmbi.1997.1370.

Baes, C. F., and R. E. Mesmer. 1976. *Hydrolysis of Cations*. New York: Wiley.

Ban, N., R. Beckmann, J.H.D. Cate et al. 2014. A new system for naming ribosomal proteins. *Current Opinion in Structural Biology* 24: 165–169. doi:10.1016/j.sbi.2014.01.002.

Bernier, C., A. S. Petrov, C. Waterbury et al. 2014. RiboVision: Visualization and analysis of ribosomes. *Faraday Discuss* 169 (1): 195–207. doi:10.1039/C3FD00126A.

Bertini, I., H. B. Gray, E. I. Stiefel, and J. S. Valentine. 2007. *Biological Inorganic Chemistry, Structure and Reactivity*. Sausalito, CA: University Science Books.

Bock, C. W., A. K. Katz, G. D. Markham, and J. P. Glusker. 1999. Manganese as a replacement for magnesium and zinc: Functional comparison of the divalent ions. *Journal of the American Chemical Society* 121 (32): 7360–7372.

Bokov, K., and S. V. Steinberg. 2009. A hierarchical model for evolution of 23S ribosomal RNA. *Nature* 457 (7232): 977–980.

Bowman, J. C., T. K. Lenz, N. V. Hud, and L. D. Williams. 2012. Cations in charge: Magnesium ions in RNA folding and catalysis. *Current Opinion in Structural Biology* 22: 262–272. doi:10.1016/j.sbi.2012.04.006.

Bray, M., T. K. Lenz, J. C. Bowman, A. S. Petrov, A. R. Reddi, N. V. Hud, L. D. Williams, and J. B. Glass. Submitted. Ferrous iron folds rRNA and mediates translation.

Brown, I. D. 1992. Chemical and steric constraints in inorganic solids. *Acta Crystallographica Section B: Structural Science* 48: 553–572.

Butcher, S. E. 2011. The spliceosome and its metal ions. *Metal Ions in Life Sciences* 9: 235–251.

Cate, J. H., A. R. Gooding, E. Podell, K. Zhou, B. L. Golden, C. E. Kundrot, T. R. Cech, and J. A. Doudna. 1996. Crystal structure of a group I ribozyme domain: Principles of RNA packing. *Science* 273 (5282): 1678–1685.

Cate, J. H., R. L. Hanna, and J. A. Doudna. 1997. A magnesium ion core at the heart of a ribozyme domain. *Nature Structural Biology* 4 (7): 553–558.

Collins, K. D., G. W. Neilson, and J. E. Enderby. 2007. Ions in water: Characterizing the forces that control chemical processes and biological structure. *Biophysical Chemistry* 128(2–3): 95–104.

Cotruvo, J. A., and J. Stubbe. 2011. Class I ribonucleotide reductases: Metallocofactor assembly and repair *in vitro* and *in vivo*. *Annual Review of Biochemistry* 80: 733–767. doi:10.1146/annurev-biochem-061408-095817.

Deras, M. L., M. Brenowitz, C. Y. Ralston, M. R. Chance, and S. A. Woodson. 2000. Folding mechanism of the Tetrahymena ribozyme P4-P6 domain. *Biochemistry* 39 (36): 10975–10985.

Derry, L. A. 2015. Causes and consequences of mid-Proterozoic anoxia. *Geophysical Research Letters* 42 (20): 8538–8546.

Diebler, H., M. Eigen, G. Ilgenfritz, G. Maass, and R. Winkler. 1969. Kinetics and mechanism of reactions of main group metal ions with biological carriers [Review]. *Pure and Applied Chemistry* 20 (1): 93–116. doi:10.1351/pac196920010093.

Doherty, A. J., and T. R. Dafforn. 2000. Nick recognition by DNA ligases. *Journal of Molecular Biology* 296 (1): 43–56.

Doudna, J. A., and T. R. Cech. 2002. The chemical repertoire of natural ribozymes. *Nature* 418 (6894): 222–228.

Draper, D. E., D. Grilley, and A. M. Soto. 2005. Ions and RNA folding. *Annual Review of Biophysics and Biomolecular Structure* 34: 221–243.

Dupont, C. L, S. Yang, B. Palenik, and P. E. Bourne. 2006. Modern proteomes contain putative imprints of ancient shifts in trace metal geochemistry. *Proceedings of the National Academy of Sciences of the United States of America* 103 (47): 17822–17827.

Ellenberger, T., and A. E. Tomkinson. 2008. Eukaryotic DNA ligases: Structural and functional insights. *Annual Review of Biochemistry* 77: 313.

Fujimoto, B. S., J. M. Miller, N. S. Ribeiro, and J. M. Schurr. 1994. Effects of different cations on the hydrodynamic radius of DNA. *Biophysical Journal* 67 (1): 304–308. doi:10.1016/S0006-3495(94)80481-3.

Grilley, D., A. M. Soto, and D. E. Draper. 2006. $Mg^{2+}$–RNA interaction free energies and their relationship to the folding of RNA tertiary structures. *Proceedings of the National Academy of Sciences of the United States of America* 103 (38): 14003.

Gutell, R. R., N. Larsen, and C. R. Woese. 1994. Lessons from an evolving rRNA: 16S and 23S rRNA structures from a comparative perspective. *Microbiological Reviews* 58 (1): 10–26.

Hansen, J. L., T. M. Schmeing, D. J. Klein, J. A. Ippolito, N. Ban, P. Nissen, B. Freeborn, P. B. Moore, and T. A. Steitz. 2001. Progress toward an understanding of the structure and enzymatic mechanism of the large ribosomal subunit. *Cold Spring Harbor Symposia on Quantitative Biology* 66: 33–42.

Harel, A., Y. Bromberg, P. G. Falkowski, and D. Bhattacharya. 2014. Evolutionary history of redox metal-binding domains across the tree of life. *Proceedings of the National Academy of Sciences of the United States of America* 111 (19): 7042–7047. doi:10.1073/pnas.1403676111.

Hribar, B., N. T. Southall, V. Vlachy, and K. A. Dill. 2002. How ions affect the structure of water. *Journal of the American Chemical Society* 124 (41): 12302–12311. doi:10.1021/ja026014h.

Hsiao, C., S. Mohan, B. K. Kalahar, and L. D. Williams. 2009. Peeling the onion: Ribosomes are ancient molecular fossils. *Molecular Biology and Evolution* 26 (11): 2415–2425. doi:10.1093/molbev/msp163.

Hsiao, C., M. Tannenbaum, H. VanDeusen, E. Hershkovitz, G. Perng, A. Tannenbaum, and L. D. Williams. 2008. Complexes of nucleic acids with group I and II cations. In *Nucleic Acid Metal Ion Interactions*, edited by N. Hud, pp. 1–35. London, UK: The Royal Society of Chemistry.

Hsiao, C., and L. D. Williams. 2009. A recurrent magnesium-binding motif provides a framework for the ribosomal peptidyl transferase center. *Nucleic Acids Research* 37 (10): 3134–3142. doi:10.1093/nar/gkp119.

Hunsicker, L. M., and V. J. DeRose. 2000. Activities and relative affinities of divalent metals in unmodified and phosphorothioate-substituted hammerhead ribozymes. *Journal of Inorganic Biochemistry* 80 (3): 271–281. doi:10.1016/S0162-0134(00)00079-9.

Jackson, V. E., A. R. Felmy, and D. A. Dixon. 2015. Prediction of the pKa's of aqueous metal ion +2 complexes. *The Journal of Physical Chemistry A* 119 (12): 2926–2939. doi:10.1021/jp5118272.

Johnson-Buck, A. E., S. E. McDowell, and N. G. Walter. 2011. Metal ions: Supporting actors in the playbook of small ribozymes. *Metal Ions in Life Sciences* 9: 175–196.

Kankia, B. I. 2003. Binding of $Mg^{2+}$ to single-stranded polynucleotides: Hydration and optical studies. *Biophysical Chemistry* 104 (3): 643–654.

Kankia, B. I. 2004. Inner-sphere complexes of divalent cations with single-stranded poly(rA) and poly(rU). *Biopolymers* 74 (3): 232–239. doi:10.1002/bip.20082.

Klein, D. J., P. B. Moore, and T. A. Steitz. 2004. The contribution of metal ions to the structural stability of the large ribosomal subunit. *RNA* 10 (9): 1366–1379.

Lavery, R., and B. Pullman. 1981. The molecular electrostatic potential, steric accessibility and hydration of Dickerson's B-DNA dodecamer d(CpGpCpGpApApTpTpCpGpCpG). *Nucleic Acids Research* 9 (15): 3765–3777.

Lee, J. Y., C. Chang, H. K. Song, J. Moon, J. K. Yang, H.-K. Kim, S.-T. Kwon, and S. W. Suh. 2000. Crystal structure of $NAD^+$-dependent DNA ligase: Modular architecture and functional implications. *The EMBO Journal* 19 (5): 1119–1129.

Lenz, T. K., A. M. Norris, N. V. Hud, and L. D. Williams. 2017. Protein-free ribosomal RNA folds to a near-native state in the presence of $Mg^{2+}$. *RSC Advances*. doi:10.1039/c7ra08696b.

Lie, L., and R. M. Wartell. 2015. Ligation of RNA oligomers by the Schistosoma mansoni hammerhead ribozyme in frozen solution RNA. 82 (2–3), 81–92.

Lykke-Andersen, J., and J. Christiansen. 1998. The C-terminal carboxy group of T7 RNA polymerase ensures efficient magnesium ion-dependent catalysis. *Nucleic Acids Research* 26 (24): 5630–5635. doi:10.1093/nar/26.24.5630.

Mähler, J., and I. Persson. 2012. A study of the hydration of the alkali metal ions in aqueous solution. *Inorganic Chemistry* 51 (1): 425–438. doi:10.1021/ic2018693.

Manning, G. S. 1969. Limiting laws and counterion condensation in polyelectrolyte solutions I. Colligative properties. *The Journal of Chemical Physics* 51 (3): 924–933. doi:10.1063/1.1672157.

Martin, J. E., and J. A. Imlay. 2011. The alternative aerobic ribonucleotide reductase of *Escherichia coli*, NrdEF, is a manganese-dependent enzyme that enables cell replication during periods of iron starvation. *Molecular Microbiology* 80 (2): 319–334. doi:10.1111/j.1365-2958.2011.07593.x.

Mayaan, E., K. Range, and D. M. York. 2004. Structure and binding of Mg(II) ions and di-metal bridge complexes with biological phosphates and phosphoranes. *JBIC Journal of Biological Inorganic Chemistry* 9 (8): 1034–1035. doi:10.1007/s00775-004-0608-2.

Morgan, B., and O. Lahav. 2007. The effect of pH on the kinetics of spontaneous Fe(II) oxidation by $O_2$ in aqueous solution—basic principles and a simple heuristic description. *Chemosphere* 68 (11): 2080–2084. doi:10.1016/j.chemosphere.2007.02.015.

Mortimer, S. A., and K. M. Weeks. 2007. A fast-acting reagent for accurate analysis of RNA secondary and tertiary structure by SHAPE Chemistry. *Journal of the American Chemical Society* 129 (14): 4144–4145.

Murray, J. B., D. P. Terwey, L. Maloney, A. Karpeisky, N. Usman, L. Beigelman, and W. G. Scott. 1998. The structural basis of hammerhead ribozyme self-cleavage. *Cell* 92 (5): 665–673. doi:10.1016/S0092-8674(00)81134-4.

Nakano, S.-i., Y. Kitagawa, D. Miyoshi, and N. Sugimoto. 2014. Hammerhead ribozyme activity and oligonucleotide duplex stability in mixed solutions of water and organic compounds. *FEBS Open Bio* 4: 643–650. doi:10.1016/j.fob.2014.06.009.

Noller, H. F., V. Hoffarth, and L. Zimniak. 1992. Unusual resistance of peptidyl transferase to protein extraction procedures. *Science* 256 (5062): 1416–1419. doi:10.1126/science.1604315.

Okafor, C. D., K. A. Lanier, A. S. Petrov, S. S. Athavale, J. C. Bowman, N. V. Hud, and L. D. Williams. 2017. Iron mediates catalysis of nucleic acid processing enzymes: Support for Fe(II) as a cofactor before the Great Oxidation Event. *Nucleic Acids Research* 45 (7): 3634–3642. doi:10.1093/nar/gkx171.

Panteva, M. T., G. M. Giambaşu, and D. M. York. 2015. Force field for $Mg^{2+}$, $Mn^{2+}$, $Zn^{2+}$, and $Cd^{2+}$ ions that have balanced interactions with nucleic acids. *The Journal of Physical Chemistry B* 119 (50): 15460–15470. doi:10.1021/acs.jpcb.5b10423.

Petrov, A. S., C. R. Bernier, B. Gulen, C. C. Waterbury, E. Hershkovitz, C. Hsiao, S. C. Harvey, N. V. Hud, G. E. Fox, R. M. Wartell, and L. D. Williams. 2014. Secondary structures of rRNAs from all three domains of life. *PLoS One* 9 (2): e88222. doi:10.1371/journal.pone.0088222.

Petrov, A. S., C. R. Bernier, C. L. Hsiao et al. 2012. RNA-magnesium-protein interactions in large ribosomal subunit. *Journal of Physical Chemistry B* 116 (28): 8113–8120. doi:10.1021/jp304723w.

Petrov, A. S., J. C. Bowman, S. C. Harvey, and L. D. Williams. 2011. Bidentate RNA-magnesium clamps: On the origin of the special role of magnesium in RNA folding. *RNA* 17 (2): 291–297. doi:10.1261/rna.2390311.

Polikanov, Y. S., T. A. Steitz, and C. A. Innis. 2014. A proton wire to couple aminoacyl-tRNA accommodation and peptide bond formation on the ribosome. *Nature Structural and Molecular Biology* 27 (9): 787–793. doi:10.1038/nsmb.2871.

Porschke, D. 1979. The mode of $Mg^{++}$ binding to oligonucleotides. Inner sphere complexes as markers for recognition? *Nucleic Acids Research* 6 (3): 883–898.

Rashin, A. A., and B. Honig. 1985. Reevaluation of the Born model of ion hydration. *Journal of Physical Chemistry* 89 (26): 5588–5593.

Robertson, M. P., and W. G. Scott. 2007. The structural basis of ribozyme-catalyzed RNA assembly. *Science* 315 (5818): 1549–1553. doi:10.1126/science.1136231.

Roychowdhury-Saha, M., and D. H. Burke. 2006. Extraordinary rates of transition metal ion-mediated ribozyme catalysis. *RNA* 12 (10): 1846–1852. doi:10.1261/rna.128906.

Scott, W. G., J. T. Finch, and A. Klug. 1995. The crystal structure of an all-RNA hammerhead ribozyme: A proposed mechanism for RNA catalytic cleavage. *Cell* 81 (7): 991–1002. doi:S0092-8674(05)80004-2.

Scott, W. G. 2007. Ribozymes. *Current Opinion in Structural Biology* 17 (3): 280–286.

Shannon, R. 1976. Revised effective ionic radii and systematic studies of interatomic distances in halides and chalcogenides. *Acta Crystallographica Section A* 32 (5): 751–767. doi:10.1107/S0567739476001551.

Steitz, T. A. 1999. DNA polymerases: Structural diversity and common mechanisms. *Journal of Biological Chemistry* 274 (25): 17395–17398. doi:10.1074/jbc.274.25.17395.

Stumm, W., and J. J. Morgan. 1996. *Aquatic Chemistry: Chemical Equilibria and Rates in Natural Waters*, 3rd ed. New York: John Wiley & Sons.

Torrents, E., P. Aloy, I. Gibert, and F. Rodriguez-Trelles. 2002. Ribonucleotide reductases: Divergent evolution of an ancient enzyme. *Journal of Molecular Evolution* 55 (2): 138–152. doi:10.1007/s00239-002-2311-7.

Travers, K. J., N. Boyd, and D. Herschlag. 2007. Low specificity of metal ion binding in the metal ion core of a folded RNA. *RNA* 13 (8): 1205–1213. doi:10.1261/rna.566007.

Ushizaka, S., K. Kuma, and K. Suzuki. 2011. Effects of Mn and Fe on growth of a coastal marine diatom Talassiosira weissflogii in the presence of precipitated Fe(III) hydroxide and EDTA-Fe(III) complex. *Fisheries Science* 77 (3): 411–424.

Vicens, Q., A. R. Gooding, A. Laederach, and T. R. Cech. 2007. Local RNA structural changes induced by crystallization are revealed by SHAPE. *RNA* 13 (4): 536–548.

Wimberly, B. T., D. E. Brodersen, W. M. Clemons, Jr., R. J. Morgan-Warren, A. P. Carter, C. Vonrhein, T. Hartsch, and V. Ramakrishnan. 2000. Structure of the 30S ribosomal subunit. *Nature* 407 (6802): 327–339.

Wolfe-Simon, F., V. Starovoytov, J. R. Reinfelder, O. Schofield, and P. G. Falkowski. 2006. Localization and role of manganese superoxide dismutase in a marine diatom. *Plant Physiology* 142 (4): 1701–1709. doi:10.1104/pp.106.088963.

Yin, Y. W., and T. A. Steitz. 2004. The structural mechanism of translocation and helicase activity in T7 RNA polymerase. *Cell* 116 (3): 393–404. doi:10.1016/S0092-8674(04)00120-5.

Zhang, C., C. Lu, Q. Wang, J. W. Ponder, and P. Ren. 2015. Polarizable multipole-based force field for dimethyl and trimethyl phosphate. *Journal of Chemical Theory and Computation* 11 (11): 5326–5339. doi:10.1021/acs.jctc.5b00562.